INVESTIGATION OF ELM DYNAMICS WITH THE RESONANT MAGNETIC PERTURBATION EFFECTS

Final Report for Period
April 1, 2009 — June 30, 2011

Prepared by
Alexei Y. Pankin and Arnold H. Kritz

Department of Physics
Lehigh University
16 Memorial Drive East
Bethlehem, PA 18015

Prepared for
United States Department of Energy
Contract No. DE-SC0000692

Final Report Grant DE-SC0000692

Prepared by

Alexei Pankin and Arnold Kritz

1 Study of anomalous transport and $E \times B$ flow shear effects in the H-mode pedestal

Several anomalous transport models have been recently implemented in the integrated modeling codes XGC0 [1] and FACETS [2, 3] using a common FMCFM interface. The FMCFM implementation of anomalous transport models has been verified against the implementation of anomalous transport in the ASTRA code [4]. The effect of flow shear on the anomalous trasnport in the H-mode pedestal has been investigated in the XGC0 code [5]. Since the XGC0 code computes the radial electric field profiles, it was natural to define the $E \times B$ flow shear rate in the XGC0 code as $\omega_{E\times B} = |RB_\theta/B_\phi \partial/\partial r(E_r/RB_\theta)|$ [6]. Here, B_θ and B_ϕ are the poloidal and toroidal components of the magnetic field, R is the major radius, and E_r is the radial component of electric field. The effect of $E\times B$ flow shear quenching is implemented through a flow shear suppression factor [7, 8]: $F_s = \beta_c/(1 + (\tau_c\omega_{E\times B})^2)$, where β_c is the calibration coefficient, and τ_c is the correlation time of fluctuations for the case without flow. After testing different channels of anomalous transport using the MMM95 module, it has been found that the resistive-ballooning component [9] is the main contributor to the anomalous transport in the plasma edge region for most of DIII-D discharges tested during the last year. It is expected that different channels of anomalous transport are suppressed at different rates. As a result, there are different coefficients β_c and different correlation times τ_c for the different drift instabilities that drive anomalous transport. It is expected that β_c is close to 1 for ITG and TEM modes and is close to 0 for ETG modes. Such difference in flow shear effects becomes apparent in the plasma edge region where the $E \times B$ flow shear plays a critical role in the formation of the H-mode pedestal. Direct first principle gyro-kinetic simulations in the pedestal region with high plasma pressure gradients remain computationally very challenging. The flow shear model calibration through direct validation of simulation results against experimental data can facilitate the development of a model for the H-mode pedestal [5, 10, 11].

Model validation is one of the major components from the very first day of this research project [4, 12]. Three sets of tokamak discharges have been identified to cover different plasma parameter regimes. The discharges include two systematic scans over plasma elongation, triangularity, and plasma current [13]. DIII-D and Alcator C-Mod, are considered: DIII-D for low B-

[1]pankin@txcorp.com

field, low density, high temperature plasmas; and C-Mod for a high B-field, high density plasmas. These validation studies are performed in close collaboration with experimentalists from General Atomics (Rich Groebner) and MIT (Jim Terry and Jerry Hughes). These validation efforts benefit from the PI participation in the HEP benchmark group organized by Jim Callen and in the FACETS validation activities. It is anticipated that the model validation will be extended to JET discharges during the last year of current funding period. In order to facilitate the experimentalist feedback on the model validation efforts, a new research blog was created [http://w3.physics.lehigh.edu/news/].

The XGC0 code has been also used in analysis mode. The effective diffusivities were derived in a form that combined with the neoclassical transport computed by XGC0, experimental profiles are reproduced. It has been found that particle and thermal pinches play an important part in the steep pedestal regions of all analyzed discharges.

2 Study of RMP effects in NSTX discharges

In collaboration with experimentalists from DIII-D (Todd Evans), UCSD (Dmitri Orlov), and ORNL (John Canik) as well as code developers from NYU (Hank Strauss), several NSTX discharges have been selected in order to study the effects of resonant magnetic perturbations (RMPs) on ELM stability. Previously, it was found that RMPs have typically destabilizing effect in the NSTX geometry, whereas RMPs have stabilizing effect in many DIII-D discharges. Understanding the differences in RMP dynamics can help in developing a comprehensive predictive model for RMP effects. In the initial simulations using the extended MHD M3D code applied to NSTX discharges, it was found that additional TRIP3D code development was necessary. The M3D code uses some supplementary information such magnetic field perturbations provided by the TRIP3D code. Necessary changes to TRIP3D have been discussed with code authors and these changes are currently being implemented. As soon as TRIP3D changes are finalized, NSTX simulations with M3D will be resumed.

3 Development of a scaling of H-mode pedestal in tokamak plasmas with type I ELMs

The XGC0 kinetic guiding-center code was used to study the neoclassical scaling of the H-mode pedestal width and height. Growth of the pedestal by neutral penetration and ionization has been limited by an ELM instability criterion computed by the ELITE MHD stability code [14]. XGC0 and ELITE coupling has been automated using the EFFIS computer science framework. First scaling study of DIII-D discharges included a scan with respect to plasma shaping, by varying the elongation by a factor of 1.4 and triangularity by a factor of 10. A scaling relation for the pedestal width and height is presented as a function of the scanned plasma parameters. Differences in the electron and ion temperature pedestal scalings are investigated [5].

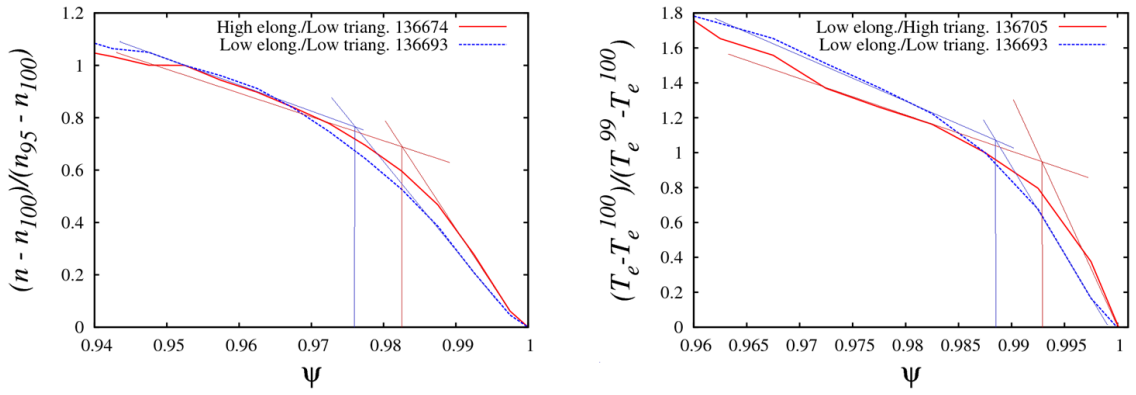

(a) (b)

Figure 1: The left panel shows the normalized plasma density profiles as a function of normalized poloidal flux for DIII-D discharges with different elongations and similar triangularities. The right panel shows the normalized plasma temperature profiles as a function of normalized poloidal flux for DIII-D discharges with different triangularities and similar elongations.

The simulation results illustrate a scaling that is qualitatively similar to some experimental observations. Fig. 1 shows the normalized plasma density and temperature profiles in DIII-D discharges with different elongations and triangularities. In XGC-0 kinetic simulations, it was found that the pedestal width is smaller for high elongation and high triangularity discharges. In the discharges considered in this study, the effect of increased elongation manifests itself in the plasma density profiles first, while the effect of increased triangularity manifests itself in the electron temperature profiles first. It has also been found that the pedestal width for the ion temperature profile is much wider than the pedestal width for the electron temperature and plasma density profiles. The pedestal height was found to be significantly larger in the discharges with larger elongation. The sensitivity of the pedestal width of density and temperature on plasma shaping can be used to test H-mode pedestal models and develop new improved discharge scenarious.

4 Divertor heat load studies

The XGC0 kinetic guiding-center code [1] was used in this study to investigate the basic kinetic neoclassical behavior of the heat and particle fluxes on divertor plates in tokamaks with a realistic divertor geometry [15–17]. The neoclassical divertor heat load fluxes were computed with the XGC0 code and a relation for the dependence of the divertor heat load width on the plasma current was derived. In the development of this relationship, effects of neutral collisions and anomalous transport were taken into account. Changes in the neoclassical divertor heat load fluxes associated with the introduction of the neutral collision and anomalous transport effects are described. For the anomalous transport, a radial random-walk is superposed in the Lagrangian neoclassical particle motion.

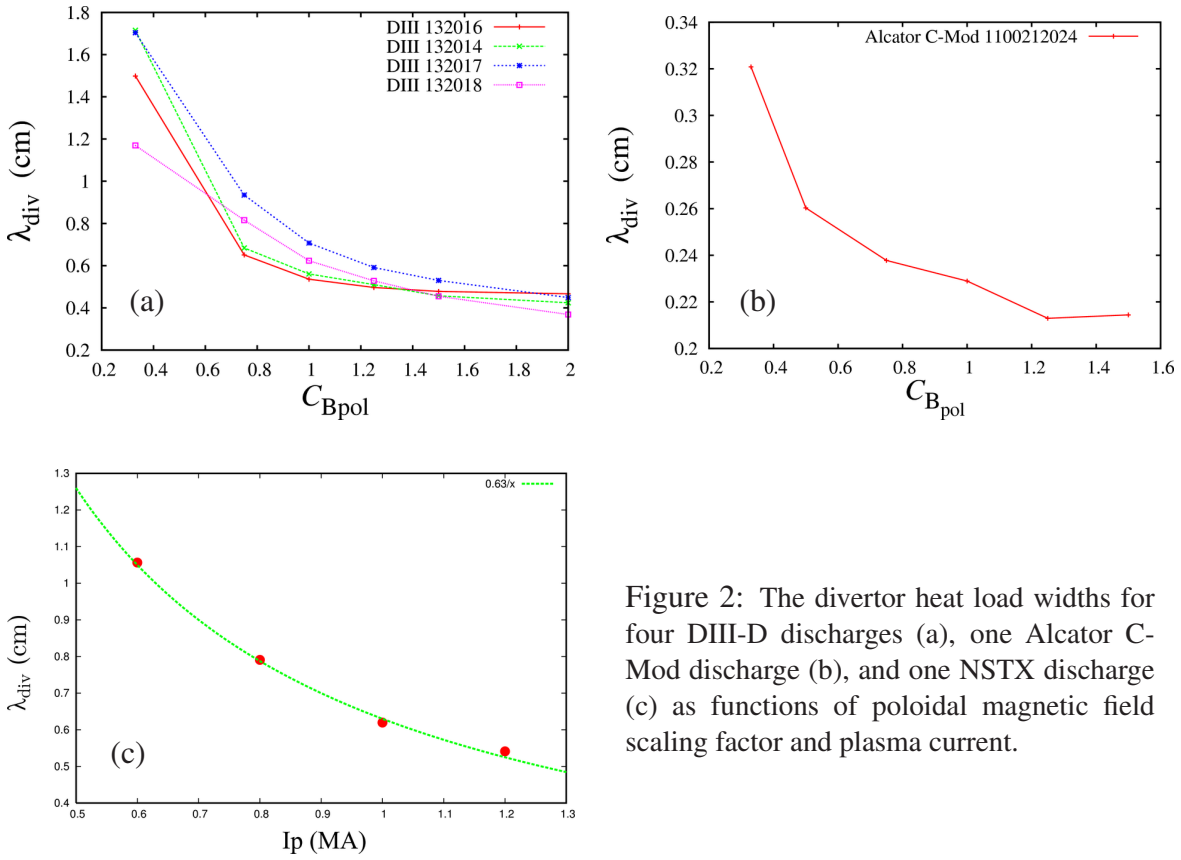

Figure 2: The divertor heat load widths for four DIII-D discharges (a), one Alcator C-Mod discharge (b), and one NSTX discharge (c) as functions of poloidal magnetic field scaling factor and plasma current.

Understanding physical effects that contribute to divertor heat load fluxes is important for experiment planning, the design of future tokamaks, and the development of new models for the SOL region. In this study, the neoclassical effects and effects due to neutral collisions and anomalous transport are investigated. A series of four DIII-D discharges representing a plasma current scan [13] was analyzed. In this series of DIII-D discharges, the total plasma current is varied from 0.51 to 1.50 MA with an approximately fixed toroidal magnetic field (B_T ≈2.1 T), plasma shape (δ ≈0.55), and normalized toroidal beta (β_n ≈2.1-2.4). In addition, one Alcator C-Mod discharge (1100212024), which was a part of Alcator C-Mod/DIII-D similarity campaign, and one NSTX discharge (128013) were analyzed. The divertor heat load widths, as functions of the poloidal magnetic field amplification factor $C_{\rm Bp}$ are shown in Fig. 2. This scaling factor is an internal numerical multiplier introduced in the XGC0 code in order to alter the initial equilibrium by scaling the poloidal flux. If the toroidal flux is not modified, the amplification factor $C_{\rm Bp}$ can be also considered as a scaling factor for the total plasma current $I_{\rm p}$. The neoclassical divertor heat load width in the Alcator C-Mod discharge is found to be approximately 2.3 mm, which is about 40% below the experimentally observed value of 3.13 mm in the base case ($C_{\rm Bp}$=1) [18]. As it will be shown below, the anomalous effects typically increase the divertor heat load width bringing the simulation results and experimental data closer to together. It has been found that the neoclassical heat load width for all four DIII-D discharges follows approximately the $1/I_{\rm p}$ dependence. There is

neither anomalous transport nor neutral effects included in these simulations. The difference in the slopes of the predicted divertor heat load widths vs C_{Bp} for different DIII-D discharges might be attributed to different collisionalities in these discharges. The differences in slopes are especially noticeable if two sets of discharges with lower (DIII-D discharges 132017 and 132018) and higher plasma densities (DIII-D discharges 132014 and 132016) are compared. This computational result on the effect of collisionality on divertor heat fluxes requires futher confirmation. In the meantime, there is no doubt that the neoclassical divertor heat load width is decreasing with increasing plasma current for all DIII-D discharges studied in this research. Correlation between the divertor heat load width and the width of radial electric field profiles in the pedestal region was found. The width of radial electric field profiles is reduced with increased plasma current. The Alcator C-Mod discharge has weaker scaling of the width of the divertor heat load with the plasma current relative to the four DIII-D discharges that were analyzed in this study. These trends reproduce the experimental observations [18–20]. The differences in neoclassical scaling of divertor heat load width might be attributed to differences in collisionality in Alcator C-Mod and DIII-D discharges. This hypothesis will be verified in future studies with the XGC0 code. The effect of neutral collisions does not significantly modify this dependence, while the inclusion of anomalous transport typically widens the divertor heat load and enhances the heat load fluxes on the divertor.

Simulation results shown in Fig. 3 demonstrate the effects of neutral collisions and anomalous transport. The dependence of the divertor heat load width is weakly affected by neutral collisions, but it can be completely modified when anomalous transport is introduced and applied uniformly for all poloidal angles. Changes to the divertor heat load width scaling are due to the ballooning nature of resistive-ballooning modes, that are likely to be major players in the region near the separatrix, are shown by the purple curve in Fig. 3. In these simulations, anomalous transport is applied in the region within 45° from the midplane. The neoclassical dependence of the divertor heat load width on the total plasma current is preserved for the high-density DIII-D discharge 132016 and almost vanished for the low-density DIII-D discharge 132018 (not shown on Fig. 3). Among all discharges studied in this research, the dependence of divertor heat load width on the current density was weakest for the DIII-D discharge 132018. The introduction of anomalous transport effects typically widens the divertor heat load width. This observation becomes evident, when the red and purple curves in Fig. 3 are compared.

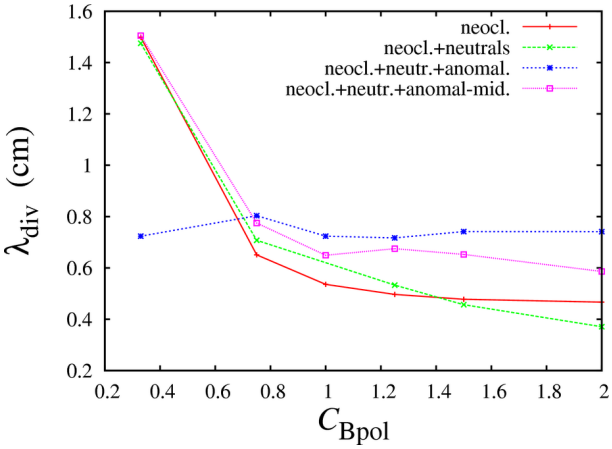

Figure 3: Effects of neutral collisions and anomalous transport on the divertor heat load width scaling in the XGC0 simulations of the DIII-D discharge 132016. The red curve shows the neoclassical scaling that does not include the effects of neutral collision and anomalous transport. The green curve shows the effect of neural collisions. The anomalous transport that is applied uniformly for all poloidal angles in used in the simulations resulted in the blue curve. The purple curve shows the divertor heat load width scaling when the anomalous transport is applied within 45° from the midplane.

References

[1] C. S. Chang, S. Ku, and H. Weitzner, Phys. Plasmas **11**, 2649 (2004).

[2] J. Cary, J. Candy, J. Cobb, R. Cohen, T. Epperly, D. Estep, S. Krasheninnikov, A. Malony, D. McCune, L. McInnes, *et al.*, SciDAC 2009, J. Physics: Conf. Series **180**, 012056 (2009).

[3] J. Cary, A. Hakim, M. Miah, S. Kruger, A. Pletzer, S. Shasharina, S. Vadlamani, A. Pankin, R. Cohen, T. Epperly, *et al.*, in *Parallel, Distributed and Network-Based Processing (PDP) (18th Euromicro International Conference)* (2010), pp. 435–442.

[4] A. Pankin, A. Pletzer, S. Vadlamani, A. Hakim, S. Kruger, M. Miah, T. Rognlien, S. Shasharina, G. Bateman, A. Kritz, *et al.*, Computer Physics Communications **182**, 180 (2011).

[5] A. Pankin, G. Bateman, A. Kritz, T. Rafiq, G. Park, S. Ku, C. Chang, and P. Snyder, in *Proc. of 51th APS DPP meeting (November 2-6, 2009, Atlanta, GA)* (2009), p. GP8.00054.

[6] T. S. Hahm and K. H. Burrell, Phys. Plasmas **2**, 1648 (1995).

[7] S. Hamaguchi and W. Horton, Phys. Fluids **B 4**, 319 (1992).

[8] K. H. Burrell, Phys. Plasmas **4**, 1499 (1997).

[9] T. Rafiq, G. Bateman, A. Kritz, and A. Pankin, Phys. Plasmas **17**, 082511 (2010).

[10] G. Bateman, A. Kritz, F. Halpern, D. McCune, R. Budny, A. Pankin, T. Rafiq, and J. Weiland, in *Proc. of Joint EU-US Transport Task Force Meeting (San Diego, CA, April 28-May 1, 2009)* (2009).

[11] A. Kritz, F. Halpern, G. Bateman, D. McCune, R. Budny, A. Pankin, T. Rafiq, and J. Weiland, in *Proc. of Joint EU-US Transport Task Force Meeting (San Diego, CA, April 28-May 1, 2009)* (2009).

[12] A. Pankin, S. Vadlamani, J. Cary, A. Hakim, S. Kruger, M. Miah, T. Rognlien, and S. Shasharina, in *Proc. of Joint EU-US Transport Task Force Meeting (San Diego, CA, April 28-May 1, 2009)* (2009).

[13] R. Groebner, A. Leonard, P. Snyder, T. Osborne, C. Maggi, M. Fenstermacher, C. Petty, and L. Owen, Nucl. Fusion **49**, 085037 (2009).

[14] P. B. Snyder, H. R. Wilson, J. R. Ferron, *et al.*, Phys. Plasmas **9**, 2037 (2002).

[15] A. Pankin, G. Park, J. Cummings, *et al.*, Problems of Atomic Science and Technology: Plasma Physics **17(N1)**, 8 (2011).

[16] A. Pankin, G. Bateman, A. Kritz, T. Rafiq, G. Park, C. Chang, D. Brunner, J. Hughes, B. LaBombard, and J. Terry, in *Proc. 52st APS DPP Meeting (November 8-12, 2010; Chicago, IL)* (2010), p. TP9.00070.

[17] J. Cummings, C. Chang, G. Park, and A. Pankin, in *Proc. 52st APS DPP Meeting (November 8-12, 2010; Chicago, IL)* (2010), p. PP9.00135.

[18] D. Brunner, B. LaBombarda, J. Paynea, and J. Terry, *Comparison of heat flux measurements by ir thermography and probes in the alcator c-mod divertor*, Journal of Nuclear Materials, in press (2011).

[19] C. Lasnier, D. Hill, T. Petrie, A. Leonard, T. Evans, and R. Maingi, Nucl. Fusion **38**, 1225 (1998).

[20] D. Hill, A. Futch, A. Leonard, M. Mahdavi, T. Petrie, D. Buchenauer, R. Campbell, J. Cuthbertson, J. Watkins, and R. Moyer, Journal of Nuclear Materials **196-198**, 204 (1992).